Flushing the Lake Littoral Region: The Interaction of Differential Cooling and Mild Winds

Cintia L. Ramón[1,2*], Hugo N. Ulloa[3,4], Tomy Doda[1,4], and Damien Bouffard[1]

[1]Department of Surface Waters – Research and Management, Eawag (Swiss Federal Institute of Aquatic Science and Technology), Kastanienbaum, Switzerland.

[2]Water Research Institute and Department of Civil Engineering, University of Granada, Spain.

[3]Department of Earth and Environmental Science, University of Pennsylvania, Philadelphia, USA

[4]Physics of Aquatic Systems Laboratory, EPFL (École Polytechnique Fédérale de Lausanne), Lausanne, Switzerland.

*Corresponding author: Cintia L. Ramón (crcasanas@ugr.es)

Key Points:

- Previous parameterizations for cross-shore discharges in the littoral region of lakes driven by differential-cooling assume calm conditions.
- Even mild cross-shore winds ($\lesssim 5$ m s^{-1}) modify the convective circulation in the lake littoral region.
- Upwind and downwind net cross-shore discharges can be predicted by the sum of the cooling and wind-driven contributions

Keywords: differential cooling, wind effects, cross-shore transport, littoral region

Abstract

The interaction of a uniform cooling rate at the lake surface with sloping bathymetry efficiently drives cross-shore water exchanges between the shallow littoral and deep interior regions. The faster cooling rate of the shallows results in the formation of density-driven currents, known as thermal siphons, that flow downslope until they intrude horizontally at the base of the surface mixed layer. Existing parameterizations of the resulting buoyancy-driven cross-shore transport assume calm wind conditions which are, however, rarely observed in lakes and thereby strongly restrict their applicability. Here we examine how moderate winds ($\lesssim$ 5 m s^{-1}) affect this convective cross-shore transport. We derive simple analytical solutions that we further test against realistic three-dimensional numerical hydrodynamic simulations of an enclosed stratified basin subject to uniform and steady surface cooling rate and cross-shore winds. We show cross-shore winds modify the convective circulation, stopping or even reversing it in the upwind littoral region and enhancing the cross-shore exchange in the downwind region. The magnitude of the simulated offshore unit-width discharges in the upwind and downwind littoral regions was satisfactorily predicted by the analytical parameterization. Our scaling expands the previous formulation to a regime where both wind and buoyancy forces drive cross-shore discharges of similar magnitude. This range is defined by the non-dimensional Monin-Obukhov length scale, χ_{MO}: $0.1 \lesssim \chi_{MO} \lesssim 0.5$. The information needed to evaluate the scaling formula can be readily obtained from a traditional set of in-situ observations.

Plain Language Summary

The flushing of the littoral region is a fundamental question for local lake managers. From a physical viewpoint, exchanges between littoral and pelagic regions are largely dominated by horizontal currents. Existing parameterizations of the cross-shore transport commonly reduce the problem to a single forcing mechanism. Wind-driven circulation is generally the main factor explaining the flushing of shallow waters in lakes. Yet, another forcing such as differential cooling resulting from a uniform surface cooling exerted on waterbodies of varying bathymetry also drives cross-shore transport. Briefly, shallow littoral waters become denser and generate a cross-shore circulation cell, with denser littoral water flowing offshore near the lake bed and lighter interior water moving onshore near the surface. However, this “thermal siphon” often co-

occurs with moderate winds ($\lesssim 5$ m s^{-1}) that drive cross-shore water exchanges of similar magnitude, limiting the applicability of existing parameterizations. Here we focus on the thermal-siphon-wind interaction regime. We derive simple analytical solutions that are satisfactorily tested against real-scale three-dimensional numerical hydrodynamic simulations of an enclosed stratified basin subject to uniform and steady surface cooling rate and cross-shore winds. Our scaling improves the estimations of the cross-shore exchange in the interaction regime.

1 Introduction

The effect of land use on downstream waters is a well-known issue. The large-scale Roman deforestation and farming in Lake Murten (Switzerland) catchment led, for instance, to its first eutrophication (Haas et al., 2019). Two millennia after, eutrophication resulting from uncontrolled nutrients loading remains a severe issue at a global scale that has fundamentally modified the lake ecology (e.g., Carpenter et al., 1998). Land-use effects also concern heavy metals (Fitchko & Hutchinson, 1975; Thevenon et al., 2011) and more recently micropollutants (Bonvin et al., 2011; Kandie et al., 2020; Perazzolo et al., 2010), microplastics (Li et al., 2018; Sighicelli et al., 2018). This list of ecologically misplanned land use ultimately affecting downstream waters could go on, and, today, lakes are well recognized as integrators of the watershed. The littoral region, as a transition zone, is particularly vulnerable to land use. Besides the already mentioned allochthonous contamination from untreated or mistreated human wastewater inflows (Timoshkin et al., 2018) and inputs of nutrients, pesticides, heavy metals, and terrestrial organic matter from runoff and/or lake tributaries (Park et al., 2009; Wei et al., 2019), the littoral region acts as an internal reactor for autochthonous processes affecting nutrient, organic matter and gas cycles. This is the case, for example, when macrophytes extensively occupy this area (e.g., James & Barko, 1991), when sediments experience different physicochemical conditions (e.g. temperature, (Hofmann, 2013) and light (e.g., Yakimovich et al., 2020)) than those in the lake interior and during events of sediment resuspension (Cyr et al., 2009; Hofmann et al., 2010). The fate and final impact of allochthonous or autochthonous compounds on the water quality depends on their residence time in the littoral region. This residence time is controlled by horizontal currents connecting the littoral and the pelagic regions (e.g., Rao & Schwab, 2007).

Horizontal exchanges result from different forcings. Wind stress acting on the lake surface is often the first investigated driver with direct (hereon wind circulation; e.g., Bengtsson, 1978) and indirect effects (e.g., basin-scale internal waves; Coman & Wells, 2012; Marti & Imberger, 2008). In the vicinity of river inflows, inertial and buoyancy forces from riverine waters are also an important localized source of horizontal exchanges (e.g., Cortés et al., 2014; Hogg et al., 2013). Finally, spatial differences in the meteorological forcing across the lake (e.g., Verburg et al., 2011) or cross-shore gradients in lake depths (Mao et al., 2019; Monismith et al., 1990) lead to differential cooling or heating that generates large horizontal exchanges. In the latter case, the shallower littoral region will heat or cool at a faster rate than the pelagic waters, yet, exposed to the same uniform air-water heat exchange rate. The resulting horizontal density gradient leads to horizontal water exchanges between the two regions. Here, we focus on periods of lake cooling, when the lake water is above the temperature of maximum density. The colder littoral region triggers density-driven currents that transport littoral water downslope and intrude horizontally at the base of the surface mixed layer (e.g. Doda et al., 2021; Fer et al., 2001). This particular type of density-driven flows are called thermal siphons (Monismith et al., 1990) and has been viewed as an important mechanism connecting the littoral and interior regions during calm conditions in lakes (Fer et al., 2001; Woodward et al., 2017) and oceanic coastal waters (e.g., Shapiro et al., 2003). For example, Fer et al. (2001) estimated from an upscaling of their local observations that the volume flux transported by thermal siphons (hereon TSs) in Lake Geneva (Switzerland) in winter is O(10) times the mean winter flow by rivers into the lake.

The flow, discharge per unit width, from the littoral region due to differential cooling depends on the magnitude of the surface buoyancy flux, B_0, and the geometry of the littoral region, as shown for example in the laboratory experiments by Sturman & Ivey (1998) and Sturman et al. (1999), and more recently in the theoretical and modeling study by Ulloa et al. (2021). Specifically, Sturman & Ivey (1998) adapted the seminal Phillips (1966) similarity solution for convective turbulent flows driven by uniform buoyancy flow in the presence of side boundaries and proposed that the steady-state discharge q_c could be estimated, as:

$$q_c = a h_{lit} (B_0 L_{SML})^{1/3}, \quad (1)$$

in which a is a proportionality coefficient varying from 0.1 to ≈ 0.4 (e.g., Doda et al., 2021; Harashima & Watanabe, 1986; Sturman & Ivey, 1998), h_{lit} is a characteristic depth of the littoral region and L_{SML} is the length of the littoral region. This scaling assumes zero wind stress; that is, calm conditions, rarely met in nature. Several field-based and modeling works have already reported that wind could block or enhance TSs (James et al., 1994; Mahjabin et al., 2019; Molina et al., 2014; Monismith et al., 1990; Roget et al., 1993; Rueda et al., 2007; Sturman et al., 1999; Woodward et al., 2017). For example, Sturman et al. (1999) reported that TSs in Australian shallow wetlands were "consistently observed" when wind speeds dropped below 3 m s^{-1}. Rueda et al. (2007) modeled differential cooling in a lagoon in Southern Spain and showed that winds weaker than 3 m s^{-1} could still slow down TSs. Woodward et al. (2017) modeled a cooling period in a reservoir in Australia and reported that "pure" TSs occur for winds lower than ~2.4 m s^{-1}, while a combined flow, mix of wind-driven and convectively-driven flow, occurred for wind speeds between 2.4-4.5 m s^{-1}. These examples suggest that there is a regime where both wind and buoyancy forces are equally important in driving the cross-shore circulation. In this regime, and depending on the wind direction, the strength of the thermal siphons could be weakened or reinforced and Eq. (1) would fail to predict the magnitude of the cross-shore discharge. A practical expression that accounts for both cooling and wind-stress effects is, thus, lacking.

Our goal is to provide a practical equation to predict the cross-shore discharge, q, due to the interaction of uniform surface cooling and mild cross-shore directed winds acting in enclosed stratified basins. Here, we couple a scaling-based analysis with numerical experiments to determine and evaluate a practical mathematical expression of the form $q_{total} = q_c + q_w$ that accounts for the cooling- (q_c) and wind-driven (q_w) contributions for the net cross-shore discharge. Our results illustrate that this simple linear expression has successful predicting skills in shallow and elongated lakes under steady forcing conditions.

2 Materials and Methods

2.1 Wind-convection interaction regime

In this study, our reference is the cross-shore flow resulting from differential cooling (Eq. 1) and we examine how mild winds modify the established convective circulation in a stratified basin. For this, the Monin-Obukhov length scale, L_{MO}, is nondimensionalized and used to define the regime of interaction between convectively and wind-driven flows:

$$\chi_{MO} = \frac{L_{MO}}{h_{SML}} = \frac{u_*^3}{kB_0 h_{SML}} = \frac{u_*^3}{kw_*^3}, \qquad (2)$$

where u_* is the surface friction velocity, defined as $u_* = (\tau_w/\rho_0)^{1/2}$ (e.g., Wüest & Lorke, 2003), τ_w is the surface wind shear stress, ρ_0 is a reference density, k (≈ 0.41) is the von Kármán constant, h_{SML} is the depth of the surface mixed-layer (hereon SML) and w_* is the convective velocity scale, defined as $w_* = (B_0\, h_{SML})^{1/3}$ (Deardorff, 1970). L_{MO} represents the depth scale over which shear dominates over convection in driving the deepening of the SML and χ_{MO} its proportion with respect to the actual SML depth. Thus, as χ_{MO} moves from zero to O(1), wind shear overcomes convection. Considering that the flow speed of TSs in sloping basins scales as $u_c = (B_0\, L_{SML})^{1/3} = w_*\, (L_{SML}/h_{SML})^{1/3}$, Eq. (2) also provides a quantification of the relative importance of wind in driving the exchange flows in littoral regions subject to surface cooling. For values of χ_{MO} tending towards zero, the effect of the wind is negligible and the exchange flow can be estimated by Eq. (1). For χ_{MO} O(1), wind-driven flows dominate the cross-shore circulation. χ_{MO} varies in temperate lakes from O(10^{-2}) to O(10) (e.g., Read et al., 2012). Here, we explore the range of χ_{MO} values delimiting the interaction regime.

2.2 Hydrodynamic model

Simulations were conducted with the three-dimensional (3D) z-coordinate RANS model MITgcm (MIT General Circulation Model, Marshall, Adcroft, et al., 1997; Marshall, Hill, et al., 1997 and details in http://mitgcm.org). MITgcm solves the Navier-Stokes equations with a finite-volume discretization and under the Boussinesq approximation. An Arakawa-C grid is used to discretize the momentum equations and a quasi-second-order Adams-Bashforth time-stepping scheme is used to advance the variables in time. Preconditioned conjugate-gradient methods are used in the 2D and 3D inversion of hydrostatic and non-hydrostatic pressure. We used the non-hydrostatic capabilities of the code and the nonlinear equation of state of McDougall et al. (2003). The advection terms in the transport equation for temperature were discretized with the non-linear 3rd order DST (direct space-time) with a flux limiter. The 3D Smagorinsky approach with a constant of 0.0005 was used to parameterize horizontal and vertical viscosities. Background vertical viscosities were set to 10^{-6} m^2 s^{-1}. Background values for the grid-dependent nondimensional lateral viscosities were set to 0.002. For a horizontal grid resolution of 2 m and a time step of 0.5 s, this is equivalent to horizontal eddy viscosity of ~ 4×10^{-4} m^2 s^{-1}. Background horizontal and vertical diffusivities for heat, K_h, and K_z, were set to 10^{-5} m^2 s^{-1} and 1.4×10^{-7} m^2 s^{-1}. No-slip conditions were applied at all lateral vertical walls and the bottom. MITgcm has been shown to successfully reproduce density-driven currents due to differential heating under ice (Ramón et al., 2021) and differential cooling in coastal sea waters (Biton et al., 2008). For reproducibility purposes, all MITgcm input files used in this study can be accessed (see link in Acknowledgments).

2.3 Lake model

To evaluate the effect of wind stress in the development of TSs in a lake, we chose an elongated trapezoidal bathymetry (Fig. 1a). This quasi 2D configuration reduces the magnitude of currents in the *y*-direction (i.e., alongshore direction, Fig. 1a) and has two symmetric littoral regions (downwind and upwind littoral regions, respectively) allowing to evaluate, in each simulation, the effect of both a favorable and opposing wind stress to the convectively-driven circulation of the lake.

Nearshore slopes of O(10^{-2}) are commonly found in lakes and depths of O(10) m are characteristic of shallow lakes. Our idealized basin holds these features. The lake's total length and width are 1800 m and 190 m, respectively. The littoral region depth, $D(x)$, increases in the x-direction from 1 m to H =16 m, the maximum depth of the lake, with a longitudinal slope S = 0.03 (Fig. 1a). The lake domain, with a total of ~ 9.8×10^6 wet cells, was discretized using a horizontally uniform Cartesian grid ($\Delta x = \Delta y = 2$ m) with vertically variable thickness (Δz). Δz increases with depth from $\Delta z = 0.05$ m within the first 2 m to cells of 0.2 m in the bottom 6 m.

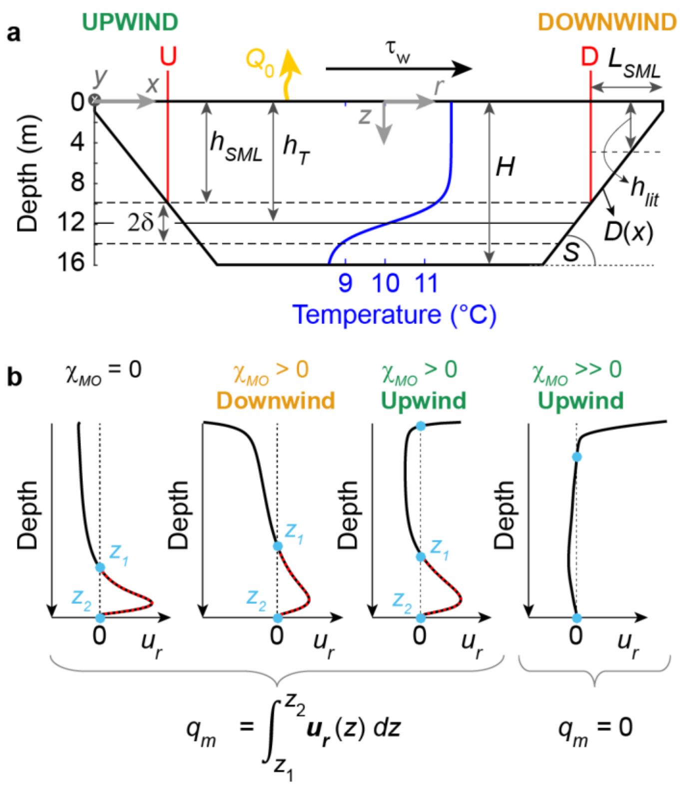

Figure 1. Model domain and calculations of offshore bottom flow. (**a**) Schematic of the model domain, initial temperature profile, and relevant length scales. Note that the vertical coordinate z has its origin ($z = 0$) at the lake surface and increases downwards, i.e., z = depth. (**b**) Schematic of possible velocity profiles in the littoral region highlighting in red the integration region for the calculations of the modeled offshore discharges q_m. Light blue dots in (**b**) mark the location of stagnation points in each profile.

In our simulations, density is a nonlinear function of temperature. The lake is initially at rest, with horizontal isotherms. The initial profile follows a hyperbolic tangent function (Eq. 3)

$$T(z) = T_b + \frac{(T_0 - T_b)}{2}\, tanh\left(\frac{h_T - z}{\delta} + 1\right), \tag{3}$$

where T_0 (= 11.7 ºC) and T_b (= 8.5 ºC) are the surface and bottom temperatures in the initial profile, and h_T (= 11. 9 m) and 2δ (= 4 m) are the fitted location of the center of the thermocline and the metalimnion width, respectively (Fig. 1a). The initial depth of the surface mixed layer is then $h_{SML,0} = h_T - \delta = 9.9$ m (Fig. 1a). The progressive deepening of the surface mixed layer was tracked by fitting Eq. 3 to the temperature profile at the lake center at each time step after removing near-surface values where temperature increases with depth ($dT/dz > 0$). Temperature boundary conditions are prescribed as adiabatic, except at the surface. The heat loss rate at the surface, Q_0, was set to 200 W m^{-2}. The surface buoyancy flux was then estimated as $B_0 = \alpha g Q_0/(\rho_e C_p)$, where α is the thermal expansivity of the surface water, g is the gravitational acceleration, ρ_e is the epilimnetic water density and C_p is the specific heat of water. For the selected Q_0, $B_0 = 5.2\times10^{-8}$ W kg^{-1} and $w_* = 8\times10^{-3}$ m s^{-1}. B_0 O(10^{-8}-10^{-7}) W kg^{-1} are typical of cooling periods in temperate lakes (e.g., Doda et al., 2021; Fer et al., 2002; Rueda et al., 2007).

Numerical experiments were initially run by only considering surface cooling until the thermally-driven cross-shore flow was stabilized. This timescale was determined a priori using the adjustment timescale introduced by Ulloa et al. (2021). The quasi-steady state should be reached at:

$$t_{onset} = \frac{2L_s}{(B_0 L_s)^{\frac{1}{3}}}\left(1 - \frac{h_p}{h_{SML}}\right)^{-\frac{1}{3}}. \quad (4)$$

Here L_s is the length of the littoral region in the sloping region ($L_s = L_{SML}$ in our bathymetry) and h_p is the depth of the plateau and here interpreted as the minimum depth of the littoral region (=1 m). With an initial L_s of ~321 m, t_{onset} should be ~7.3 h. Once TSs were fully developed and reached a quasi-steady state, constant wind stress, τ_w, in the direction of the main lake axis (E-W direction) was applied with a ramp-up period of 1 h. Together with the zero wind stress case (run 0 in Table 1), we tested through a parametric study the effect of 6 different values of τ_w, increasing from O(10^{-4}) to (10^{-2}) N m^{-2} which resulted in χ_{MO} values increasing from 0 to ~ 0.5

(runs 1-6 in Table 1). To evaluate the effect of the wind alone and to test the "additive assumption", i.e. that the net transport can be expressed as a linear superposition of the wind- and thermally-driven cross-shore transport, a set of 6 simulations (W-runs in Table 1) was conducted in which the lake was only forced with a surface wind stress. Details of the modeled flows for the W-runs and the resulting fit with the wind scaling (see Section 2.5) are included in Fig. S1 in the supporting information.

Table 1. Run cases. Initial χ_{MO} values and wind forcing.

Run	χ_{MO}	u_* (m s^{-1})	τ_w (N m^{-2})	u_{10} (m s^{-1})[a]
0	0	0	0	0
1	1×10^{-3}	6.0×10^{-4}	3.6×10^{-4}	0.04
2	2.8×10^{-2}	1.8×10^{-3}	3.2×10^{-3}	0.54
3	6.6×10^{-2}	2.4×10^{-3}	5.8×10^{-3}	1.09
4	1.3×10^{-1}	3.0×10^{-3}	9.0×10^{-3}	1.82
5	3.1×10^{-1}	4.0×10^{-3}	1.6×10^{-2}	3.58
6	5.3×10^{-1}	4.8×10^{-3}	2.3×10^{-2}	4.33
W1	-	6.0×10^{-4}	3.6×10^{-4}	0.04
W2	-	1.8×10^{-3}	3.2×10^{-3}	0.54
W3	-	2.4×10^{-3}	5.8×10^{-3}	1.09
W4	-	3.0×10^{-3}	9.0×10^{-3}	1.82
W5	-	4.0×10^{-3}	1.6×10^{-2}	3.58
W6	-	4.8×10^{-3}	2.3×10^{-2}	4.33

[a] u_{10} is the wind velocity at 10 m height above the water surface calculated as $u_{10} = [\tau_w /(\rho_{air}C_d)]^{½}$, where ρ_{air} is the air density (= 1,23 kg m^{-3}) and the wind drag coefficient, C_d, is a function of u_{10} (Wüest & Lorke, 2003).

2.4 Calculation of offshore flows

Near-bed offshore flows were calculated, over time and for the entire basin, from the modeled width-averaged radial velocity field as

$$q_m(t,r) = \int_{z_1}^{z_2} \boldsymbol{u_r}(t,r,z)dz. \tag{5}$$

Here u_r is the width-averaged radial velocity (r = 0 at the lake center, Fig. 1a). The sign of u_r is switched so that radial velocities are positive if directed offshore. z_1 and z_2 mark the limits of the integration over depth (Fig. 1b). For the half of the lake located downwind, wind stress reinforces the convectively-driven circulation and, as a result, a two-layered exchange flow develops in the littoral region. Depth z_1 is the shallowest stagnation depth within the water column, that is $u_r(t,r, z = z_1) = 0$ m s^{-1}. Point z_2 is the depth of the lake bed at locations shallower than h_{SML} or, otherwise, the second stagnation depth from the lake surface (Fig. 1b). For the other half of the lake, the upwind region, the cooling-driven circulation and wind-driven circulation act in opposite directions. If the wind is only able to arrest TSs, a three-layer exchange flow develops in the littoral region, with a surface (wind-driven) and near-bed(convectively-driven) current directed offshore, and an intermediate onshore current (Fig. 1b). Depths z_1 and z_2 are, in this case, the limits of the bottom convectively-driven current, which correspond to the second and third (or the bottom of the lake at locations shallower than h_{SML}) stagnation depths from the surface, respectively.

We further use z_1 and z_2 to remove offshore circulation developing at the thermocline region, which is not the subject of this study. Specifically, z_1 should be shallower than h_{SML} and more than 2/3 of the layer should be above h_{SML}, that is $|h_{SML}-z_1| > 2/3\ |z_2-z_1|$. If this criterion is not met, q_m is set to 0 m^2 s^{-1}. If the wind-driven circulation can overcome the convectively-driven circulation, a two-layer flow exchange develops in the littoral region, with a bottom current directed onshore, and thus $q_m = 0$ m^2 s^{-1} (Fig. 1b). Note that here, we are evaluating the effect of the wind on the intensity of TSs, so that q_m is the proportion of the offshore flow transported by near-bed currents. In the downwind region q_m is equal to the total offshore transport in the littoral region (= ½ $\int |u_r| dz$). In the upwind region, however, q_m is lower than the total offshore transport since we are not integrating the wind-driven near-surface currents (Fig. 1b).

2.5 Combined wind and convective cross-shore transport

We consider steady wind stress along the main axis of a lake and make the following assumptions: (1) vertical viscosity, ν_z, is uniform within the SML and (2) slope effects are negligible (slope $S << 1$). We also recall the no-slip bottom boundary condition and flow continuity. Given such background conditions, the associated wind-driven steady-state velocity profile in the littoral region can be expressed as (e.g., Cormack et al., 1975)

$$u(x,z) = \frac{\tau_w}{\rho_0 \nu_z}\left(\frac{3}{4}\frac{(D(x)-z)^2}{D(x)} - \frac{D(x)-z}{2}\right), \quad (6)$$

where $D(x)$ is the maximum water column depth at a given x location within the littoral region (Fig. 1a). The velocity profile in Eq. 6 changes sign at a depth $z_0(x) = 1/3D(x)$. The wind-driven offshore flow, $q_w(x)$, can then be estimated by integrating Eq. 6 from $z_0(x)$ to $D(x)$.

$$q_w(x) = \int_{z_0}^{D(x)} u(x,z)\, dz = \frac{\tau_w}{\rho_0 \nu_z}\frac{D(x)^2}{27}. \quad (7)$$

Thus, within the littoral region, q_w is maximal at its offshore end, where $D(x) = h_{SML}$.

We assume that net cross-shore transport can be expressed as a linear superposition of surface cooling and wind effects. The validity of this linear assumption is tested and discussed in section 3.3. Therefore, offshore discharge per unit width is estimated as:

$$q_{total} = q_c + q_w, \quad (8)$$

where q_c is defined in Eq. 1 and q_w is positive (directed offshore) at depths deeper than $z_0(x)$ on the side where the wind blows towards the littoral. Since we are interested in the discharge transported by offshore bottom currents, we will set q_{total} = 0 m^2 s^{-1} whenever ($q_c + q_w$) < 0 m^2 s^{-1}. The latter occurs when the wind-driven circulation overcomes the convectively-driven circulation in the upwind littoral region (Fig. 1b).

The different expressions for the flow scaling (q_c, q_w, and q_{total}) were compared with the modeled flows, q_m (Eq. 5) in profiles U and D (Fig. 1a), located at the initial offshore end of the upwind and downwind littoral regions, respectively. Given that those are fixed profiles, the vertical length scales in the calculations of q_c and q_w are kept constant. For computing the convective scaling (Eq. 1), $h_{lit} = h_{lit,0}$, which is the average depth of the initial mixed littoral region. For the wind scaling (Eq. 7), $D = h_{SML,\,0}$, which is the initial SML depth. The forcing length scale, L_{SML}, however, grows as the SML deepens over time (e.g, Doda et al., 2021).

3 Results

3.1 Upwind and downwind lake circulation

The characteristic cross-shore circulation cell associated with TSs in the littoral region of a lake is observed for the runs with the smallest χ_{MO} values (see black and red lines for $\chi_{MO} = 0$ and $\chi_{MO} = O(10^{-3})$, respectively, in Fig. 2). Density currents flow downslope, leading to positive radial velocities near the littoral bed. A return flow, with negative radial velocities, develops in the upper part of the water column to fulfill continuity. This characteristic velocity profile is observed in both littoral regions (Figs. 2a,b). As χ_{MO} increases, and reaches magnitudes above $O(10^{-2})$, the thermal siphon in the upwind side tends to be arrested, as shown by the decreasing near-bed radial velocities (green line in Fig. 2a). For $\chi_{MO} \gtrsim 0.07$ ($\tau_w \gtrsim 0.0058$ N m^{-2}, $u_{10} \gtrsim 1$ m s^{-1}) our simulations already predict a reversed circulation in the upwind side, with bottom currents directed onshore ($u_r < 0$ m s^{-1} in Fig. 2a). By contrast, the cross-shore exchange is amplified in the downwind littoral region since the wind and thermally-driven circulation work in phase, resulting in an enhancement of near-bed currents (Fig. 2b). The depth where the velocity profile changes sign also becomes shallower as χ_{MO} (and so wind stress) increases. For the two simulations with the highest χ_{MO}, this depth approaches the value of z_0 (= 1/3D(x); ~ 3.3 m in Fig. 2b) predicted by Eq. 3 (see Sect. 2.2), suggesting that the wind was the predominant flow driver.

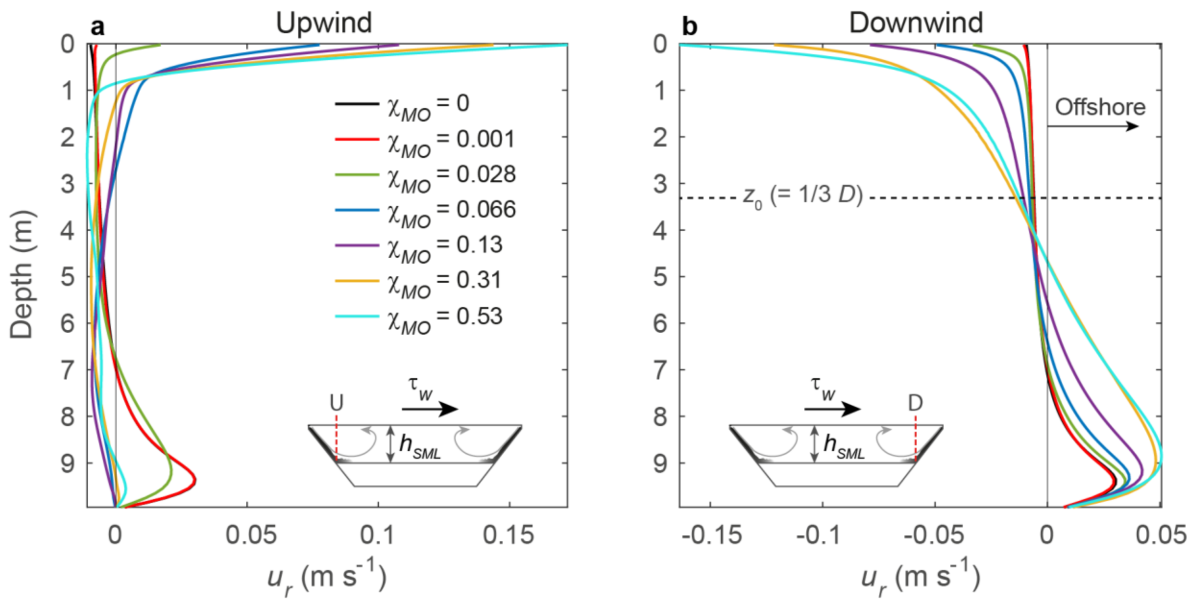

Figure 2. Velocity profiles in the upwind and downwind littoral regions. Example of time-averaged radial velocity profiles in the (**a**) upwind and (**b**) downwind littoral regions, where D(x) = 9.9 m (locations U and D, respectively), for runs 0 to 6 in Table 1. The velocity is positive if directed offshore. Averaging period from t = 20 h to t = 36 h.

3.2 Flow discharges from the littoral region

The wind-driven changes in the circulation pattern reported in Section 3.1 impacted the near-bed transport of littoral water towards the lake interior (Fig. 3). For the zero wind-stress case (χ_{MO} = 0), there is a radial symmetry in the q_m signal (Fig. 3a). On each sloping side, the maximum flow rate is observed near the end of the littoral region (blue dotted lines in Fig. 3), and from there, it decreases both towards the lateral boundaries and the lake center. Once wind stress is applied over the lake (χ_{MO} > 0), the upwind side experiences two main modifications. First, the area with near-bottom offshore discharge (q_m > 0 m^2 s^{-1}) decreases (e.g., Fig. 3c).

Second, the location of the maximum flow rate is displaced offshore (e.g., Figs. 3d,e). These two effects are intensified as the magnitude of the wind stress increases, especially the reduction of q_m (Fig. 3f,g). In the downwind region, the area with $q_m > 0$ m^2 s^{-1} expands towards the lake interior as the stress increases. Still, maximum values remain centered around the end of the littoral region (Figs. 3a-f), except for the strongest wind (Figs. 3g).

As the magnitude of the applied wind stress increases, the magnitude of the near-bed offshore flow increases (decreases) with respect to the wind-free case in the downwind (upwind) region (Fig. 3). These trends are shown in the time series of q_m at locations U and D (Fig. 4). Downwind, modeled flows subjected to the highest wind stress rapidly increased to values that quadruple on average those in the wind-free case. Upwind, the modeled flow rapidly decreased and represents, for $\chi_{MO} \gtrsim 0.07$, less than 20% of the flow in the wind-free case.

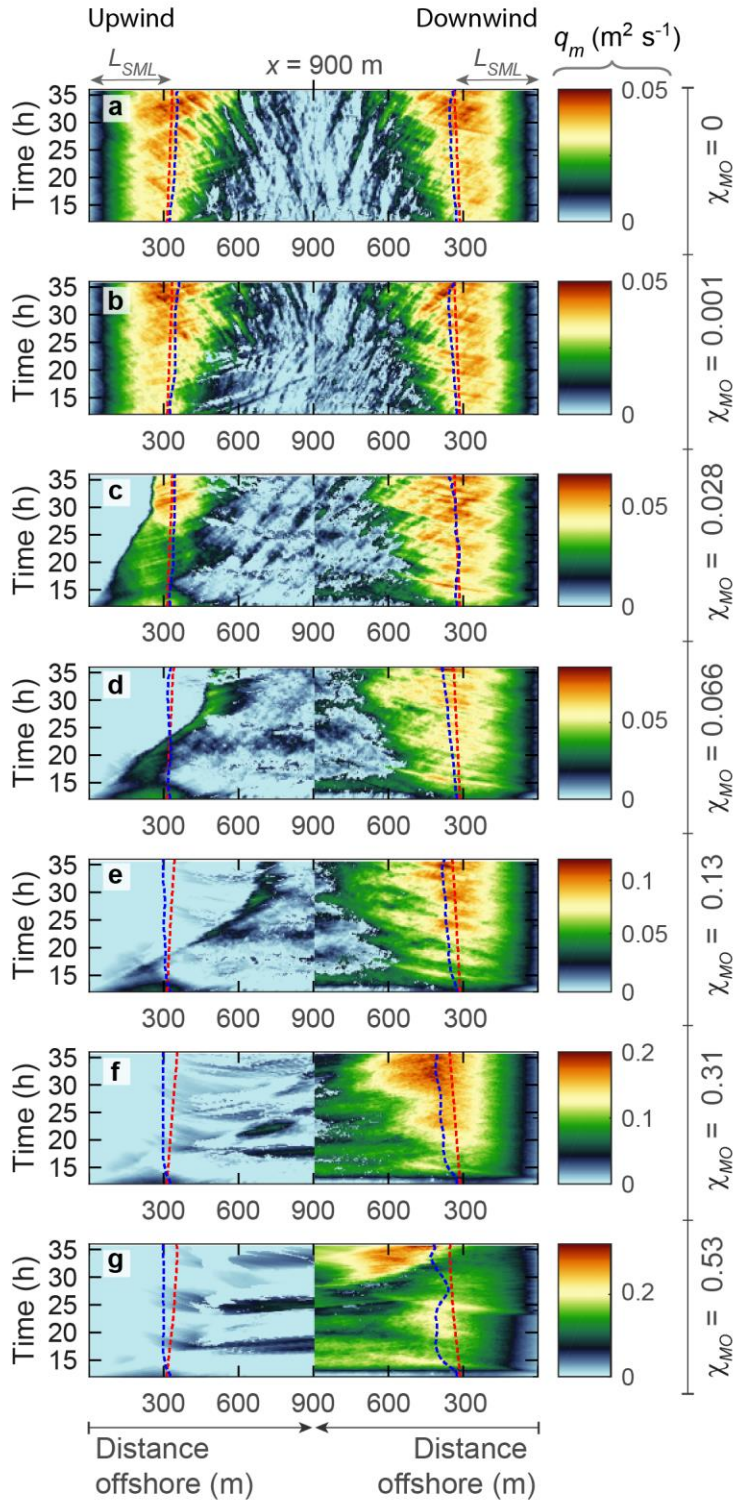

Figure 3. Space-time modeled bottom offshore unit-width discharges, q_m, for different χ_{MO}. Results of (**a-g**) runs 0 to 6 in Table 1. Offshore discharges are positive if directed towards the lake center, located at x = 900 m, where the offshore direction reverses. As χ_{MO} increases, the

basin-scale wind circulation dominates over the convective circulation, and bottom offshore discharges are restricted to the downwind region. Dashed blue and red lines show the 6h-smoothed end of both littoral regions calculated from an equilibrium density profile (red line) where density is redistributed to attain the minimum potential energy in the system (Winters et al., 1995), and from the actual intersection of h_{SML} with the lake bathymetry (blue line). Blue lines consider both the scouring of h_{SML} due to intrusions of gravity currents and the wind-driven tilting of the isotherms. Wind stress over the lake starts at t=12 h. Note the increasing range of the colorbar from (**a**) to (**g**).

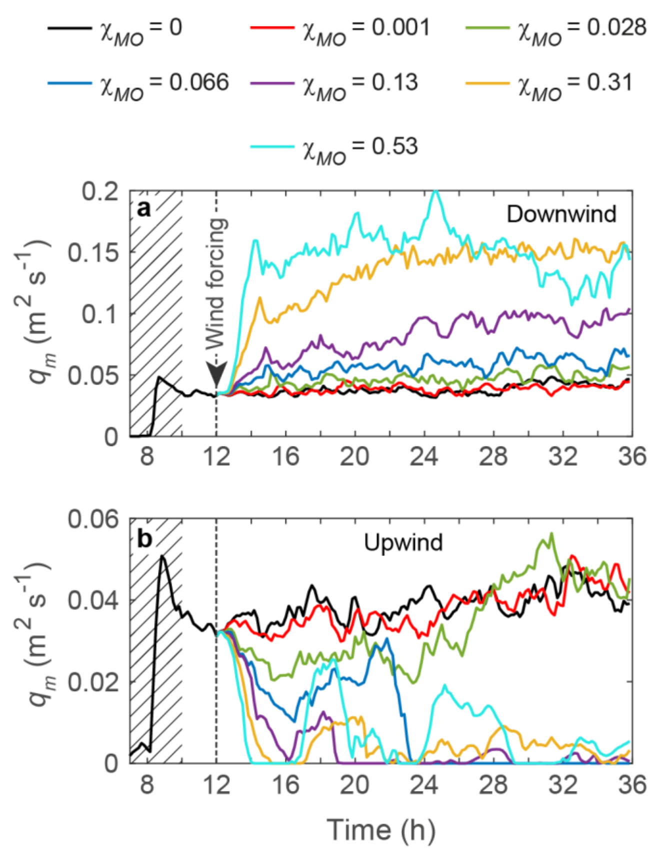

Figure 4. Time series of modeled flows for different χ_{MO}. Profiles (**a**) D (downwind) and (**b**) U (upwind). Grey oblique lines mark the TS-development period. Wind stress over the lake starts at t=12 h.

3.3 Parameterization of discharge from the littoral region

The model results confirm that the wind can either enhance or block TSs. This section illustrates that the assumption of linearity between convectively- and wind-driven effects on the cross-shore exchange is reasonable over the studied χ_{MO} range. Figure 5a shows the time-averaged modeled flows in profiles U and D (red open and closed squares, respectively) together with the results from the three different scalings. Recall that there is a proportionality coefficient, a, in the convective flow scaling (Eq. 1) and that vertical viscosity, ν_z, appears in the scaling for the wind-driven discharge (Eq. 7). The linear assumption implies that the values of both a and ν_z are independent of the applied wind stress, and thus, that one unique value should be used for the parameter space here examined.

The value of a was obtained by fitting Eq. 1 to the modeled flows for the wind-free case, which results in $a = 0.29 \pm 0.01$. This value is within the expected range predicted in laboratory experiments (Harashima & Watanabe, 1986). The time-averaged discharge q_c, predicted with Eq. 1, is shown as a function of χ_{MO} in black in Fig. 5a; q_c remains almost constant through the range of χ_{MO}. This was expected given a maximum difference in the deepening of the SML during the time-averaging period of only 0.5 m between simulations. With a longitudinal slope of 0.03, this deepening difference resulted in a difference of L_{SML} of ~ 20 m. Since q_c is a function of the length of the littoral region to the power of ⅓, differences in the rate of SML deepening among simulations could only introduce O(10^{-3}) $m^2\ s^{-1}$ differences in the estimated convective flows during the time-averaging period.

The value of ν_z was obtained by fitting Eq. 7 to the modeled flows in the downwind littoral region in the simulations where the lake surface was only subjected to wind stress (W-simulations, in Table 1). This fit leads to a value for ν_z of $6.0 \pm 0.4 \times 10^{-4}\ m^2\ s^{-1}$ (see Fig. S1 in the supporting information). This value of ν_z is of the same order of magnitude of the modeled viscosities within the SML and of the same order of magnitude as measured vertical viscosities in lake and oceanic SMLs for the same range of wind stresses (e.g., Bengtsson, 1973; Santiago-Mandujano & Firing, 1990). Eq. 7 predicts a linear increase of the wind-driven offshore flows in the downwind litoral region as χ_{MO} and the applied stress increases, as indicated by the blue line in Fig. 5a. Given that q_c remained almost constant among simulations, the addition of convectively- and wind-driven effects in the downwind region (closed light blue circles in Fig. 5a) is reflected as an offset to the discharges predicted by Eq. 7. In the upwind region, the subtraction of the two effects predicts reversed flows, q_{total} = 0 m^2 s^{-1}, for $\chi_{MO} \gtrsim 0.1$ ($\tau_w \geq 9 \times 10^{-3}$ N m^{-2}, open light blue circles).

While the interaction of TS and wind-driven currents is fundamentally a non-linear problem, our simple linear approach has useful predicting skills. In our worst-case scenario, the deviation between modeled and predicted flows remained < 25% on the downwind side (Fig. 5b).

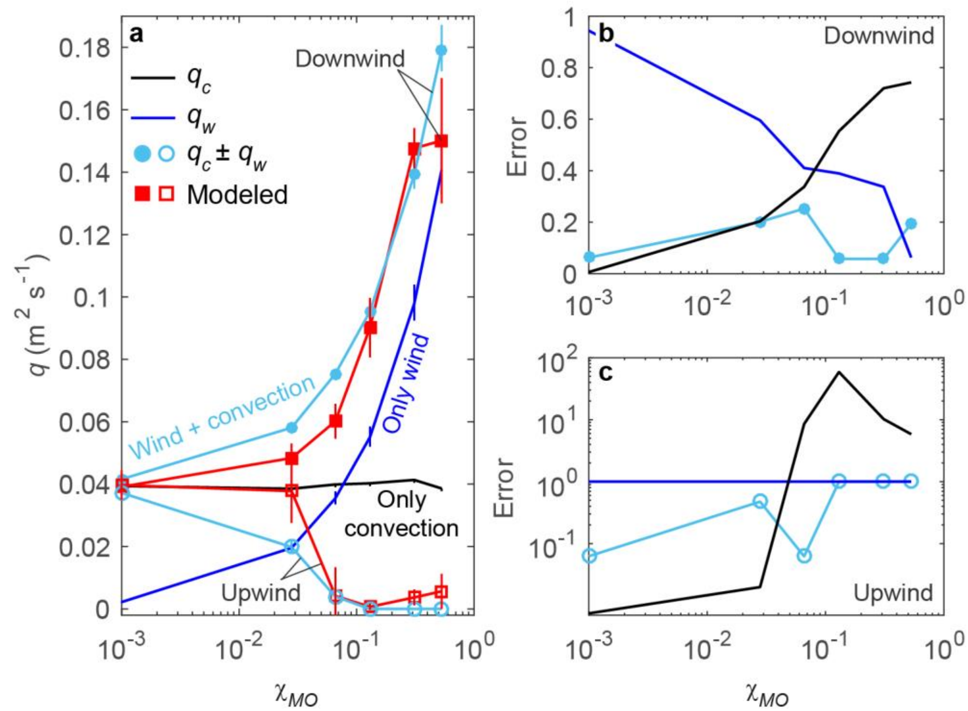

Figure 5. Modeled *vs.* predicted flows for different χ_{MO}. (**a**) Time-averaged predictions with the convective (black), wind-driven (dark blue), and additive (linear) scaling (light blue) *vs.* modeled (red) flows in profiles U (upwind, open symbols) and D (downwind, closed symbols). The time-averaging period is t=20-36 h. Vertical lines on the modeled values show ± one standard deviation. Vertical lines in the different scaling curves show the uncertainty coming from the 95 confidence interval of the fitting coefficient a (= 0.29 ± 0.006) in Eq. 1 and $\nu_z = 6.06 \times 10^{-4} \pm 3.6 \times 10^{-5}$ m^2 s^{-1} in Eq. 7. (**b-c**) Non-dimensional error for the different scaling predictions in (**a**). Relative error = $|q_m\text{-}q_\beta|/q_m$, where q_β refers to any of the tested scalings (q_c, q_w and q_{total}). Recall that $q_w = 0$ m^2 s^{-1} in the upwind region.

4 Discussion

4.1 Field application: Lake Rotsee

Rotsee (47.06 °N, 8.31°E and maximum depth of 16 m, Fig. 6a) is a Swiss dimictic perialpine elongated lake. Doda et al. (2021) studied the seasonal occurrence of TSs in this lake. By deploying a chain of thermistors and an upward-looking Acoustic Doppler Current Profiler in the north-eastern littoral region of the lake (point A in Fig. 6a) during a year-long field study, they were able to detect the presence of TSs (see details of field measurements and TS detection procedure in Doda et al. (2021)). The authors obtained a value for the proportionality coefficient $a = 0.34 \pm 0.02$ (Eq. (1)) yet highly scattered ($R^2 = 0.27$). The lake is characterized by its calm conditions; still, cross-shore flows were identified as wind-driven for almost 10% of the days with measurements (Doda et al., 2021). We applied our framework to the days with cross-shore flows identified as TSs or wind-driven flows by Doda et al. (2021). We further restrict our study to night-time flushing events, when radiative forcing is zero. Doda et al. (2021) observed indeed an intensification of cross-shore flows at the start of the heating phase, and this unsteady effect is not investigated in our study. To calculate q_c, we followed Doda et al. (2021), using their proportionality coefficient and setting $h_{lit} = 1.7$ m (the average depth of the littoral region onshore of point A). To calculate q_w, we set $D = 4.2$ m, the lake depth at the measured location (point A, Fig. 6a). B_0 during the cooling periods was on average O(10^{-8}) W kg^{-1}, with an O(10^{-9}-10^{-7}) W kg^{-1} range. τ_w ranged from O(10^{-8}) to O(10^{-2}) N m^{-2}. Due to the progressive deepening of the surface mixed layer, L_{SML} increased from ~200 m in June to ~800 m in December (Doda et al., 2021).

By adding days with cross-shore flows defined as wind-driven by Doda et al. (2021), predicted unit-width discharges further deviate from the 1:1 relationship with the convective scaling, q_c, and $R^2 < 0.1$ (black open circles in Fig. 6b). Examples of such wind-driven events are shown in Figs. 6c,i,j, where the convective scaling (black lines) fails to predict the magnitude of the measured (orange signal) offshore discharges. Predicted offshore discharges including the effect of the wind in the scaling (blue lines) closely follow the measured ones on those same days. Other examples of days when TSs interacted with wind-driven currents are shown in Figs. 6d-h. For example, Figs. 6f,h show days when the wind forcing effectively weakened TSs. Overall, including wind effects increased the goodness of predictions for unit-width discharges in the littoral region in Rotsee ($R^2 = 0.43$, Fig. 6b).

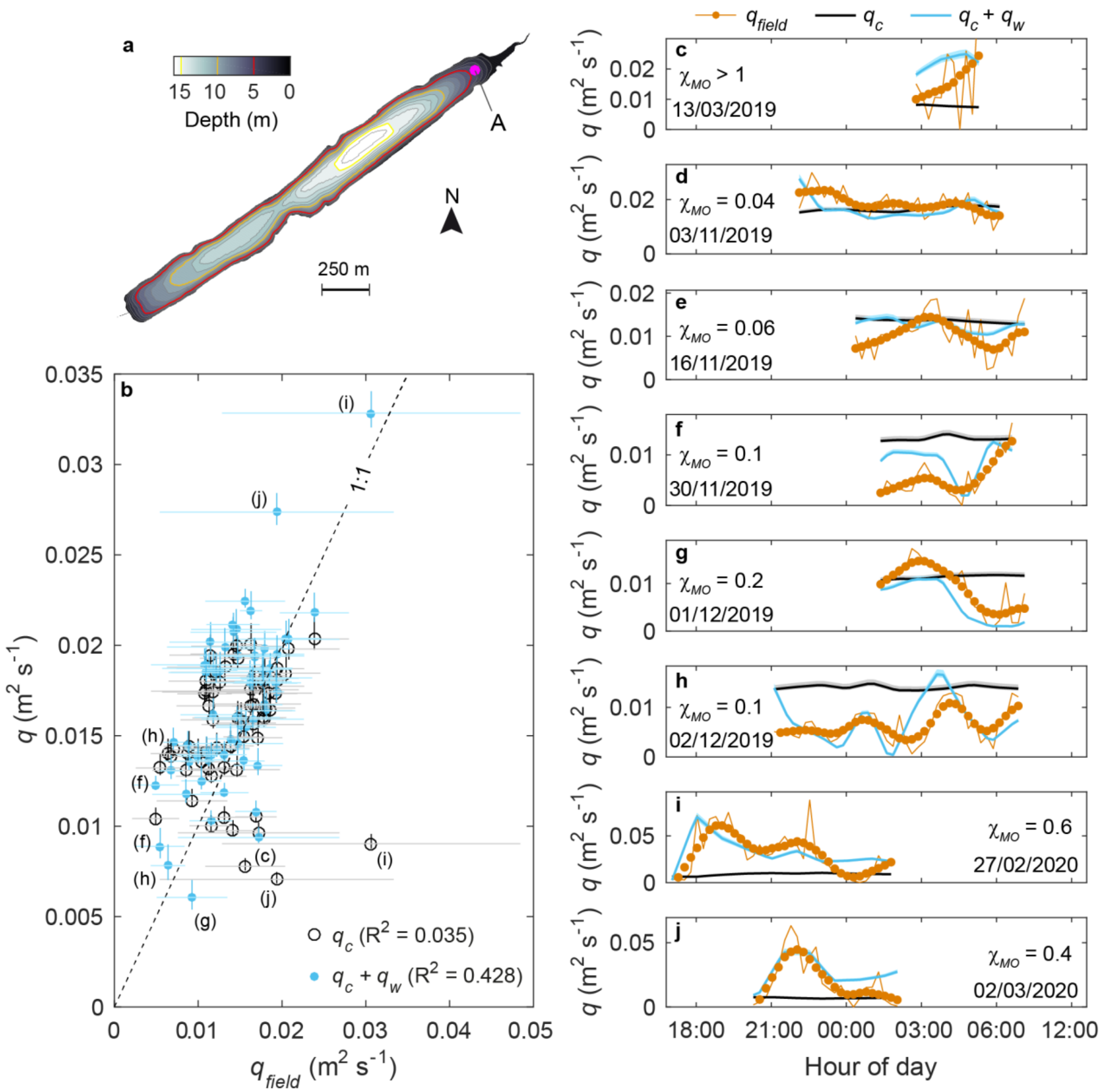

Figure 6. Predicted *vs.* measured unit-width discharges during cooling periods in Rotsee. (**a**) Bathymetry of Rotsee indicating the measurement location (point A). (**b**) 1:1 relationship of daily averages of measured (q_{field}) and predicted unit-width discharges for the convective scaling (q_c, Eq. (1)) and the additive (linear) scaling for wind and convection (q_c+q_w, Eq. (8)) for 66 days in Rotsee. Discharges were averaged over each daily cooling period. Vertical and horizontal lines crossing the open and closed circles show the 95% confidence interval of proportionality coefficient a (= 0.34 ± 0.02; Doda et al., 2021) and v_z (= $6.06 \times 10^{-4} \pm 3.6 \times 10^{-5}$ m^2 s^{-1}, see Supporting Information) and ± 1 standard deviations of q_{field}, respectively. (**c-j**) Example of

measured and predicted unit-width discharges and average χ_{MO} during eight different flushing events in Rotsee. Letters beside some of the symbols in (**b**) correspond to the cooling periods shown in panels (**c**)-(**j**). A 3h-smoothing (filled orange circles) was applied to all the unit-width discharge signals.

4.2 The interaction regime

A non-dimensional Monin-Obukhov length scale has been used in this study to define the interaction regime between convection and wind in the flushing of lakes' littoral regions. Our results indicate that this regime occurs for values of χ_{MO} in the range $0.1 \lesssim \chi_{MO} \lesssim 0.5$. Indeed, for this range of χ_{MO}, unit-width discharges are better predicted in our simulations and Lake Rotsee (Fig. 6) when both the wind- and convectively-driven transport scalings are included (Eq. 5, Fig. 5). Rueda et al. (2007) reported that offshore winds of 3 m s^{-1} were able to weaken TSs in La Caldera (37ºN, 3ºW). For $B_0 \sim 7\times 10^{-8}$ W kg^{-1} and h_{SML} ~10 m during their simulated period (calculated from reported w_* and h_{SML} values in Rueda et al. (2007)), a 3 m s^{-1} wind results in $\chi_{MO} \sim 0.1$. Sturman et al. (1999) reported evidence of TSs in well-mixed 3-m-deep Lake Yangebup (32°S, 115°E) when winds were below 3 m s^{-1}. For h_{SML} ~3 m (well-mixed lake), and their reported values of heat loss rate of ~200 W m^{-2} ($B_0 \sim 8\times 10^{-8}$ W kg^{-1}), this situation corresponds to $\chi_{MO} \lesssim 0.4$. Both examples are consistent with our defined interaction regime based on χ_{MO}.

Other parameters have been suggested in the literature to evaluate this interaction. For example, studies on cross-shore exchanges due to differential cooling in the inner shelves of oceanic coastal waters commonly use the horizontal Richardson number, Ri_x (e.g., Horwitz & Lentz, 2014; Mahjabin et al., 2019, 2020):

$$Ri_x = \frac{g\ D(x)^2}{\rho_0 u_*^2}\frac{\partial \rho}{\partial x}, \tag{9}$$

where $\partial\rho/\partial x$ is the cross-shelf density gradient. The horizontal Richardson number (Eq. 9) is inversely proportional to χ_{MO} (Eq. 2). For a shear time scale, $t_{shear} \sim L_{SML}\, k\, u_*^{-1}$, and in the absence of horizontal advection of heat, the horizontal density gradient built by differentially cooling over the wedge region will increase up to (e.g., Horwitz & Lentz, 2014):

$$\frac{\partial\rho}{\partial x} = -\frac{B_0\rho_0}{g}\frac{S}{D(x)^2}\, t_{shear} \approx -\frac{B_0\rho_0 h_{SML} k}{g u_*}\frac{1}{D(x)^2}, \qquad (10)$$

where the cross-shore slope $S \approx h_{SML}/L_{SML}$. Reordering Eq. 10 to obtain a relationship for $B_0 h_{SML} u_*^{-1}$ and substituting it into Eq. 2, it follows that $\chi_{MO} \approx Ri_x^{-1}$. Our simulations confirm indeed this approximate relationship (see Fig. S2 in Supporting Information).

Horwitz & Lentz (2014) explored through numerical simulations the effect of the presence of a horizontal density gradient on the circulation driven by cross-shore directed winds. For absolute values of $|Ri_x| < 1$ ($|\chi_{MO}| > 1$), they showed that the main effect of the presence of a horizontal density gradient is to enhance or decrease vertical shear by strengthening vertical stratification or destabilizing the water column, respectively. For $Ri_x > 1$ ($\chi_{MO} < 1$), however, Horwitz & Lentz (2014) hypothesized that the horizontal density gradient had an increasing contribution in directly driving the cross-shore circulation. This was eventually confirmed by Mahjabin et al. (2019) in their field experiments in the Rottnest continental shelf (32ºS, 115ºE, Australia), where they observed that strong thermally-driven dense shelf water cascades develop when $Ri_x \gtrsim 2$ ($\chi_{MO} \lesssim 0.5$).

Woodward et al. (2017) applied in their numerical simulations of the hydrodynamics of Lake Argyle (16ºS, 128ºE) the parameter B introduced by Cormack et al. (1975) to measure the relative magnitude of shear and buoyancy forces in shallow rectangular cavities with differentially heated end-walls:

$$B = \frac{L\tau_w}{h^2 \Delta T \alpha g}. \qquad (11)$$

Here, L and h correspond to the length and depth of the cavity, respectively, and ΔT is the temperature difference between the differentially-heated end-walls. Applying this scaling to the littoral region of lakes with S <<1 and assuming a constant horizontal density gradient $\partial\rho/\partial x \sim \rho_0 \alpha \Delta T\, L^{-1}$, expression (11) reduces to $B \approx \chi_{MO} \approx Ri_x^{-1}$. Woodward et al. (2017) reported that for values of $0.1 \lesssim B \lesssim 0.5$, the cross-shore exchange was driven by a combination of wind and horizontal convection, while for values of $B \lesssim 0.1$ and $B \gtrsim 0.5$, the exchange was mainly driven by convection and wind shear, respectively. Given that $B \approx \chi_{MO}$, this regime delimitation is consistent with our simulations. The upper and lower bounds of the interaction regime are however approximate, given the dependency of the convective velocity on the longitudinal slope ($\sim S^{-1/3}$). The validity of parameter χ_{MO} as a regime delimiter is nontrivial. χ_{MO} does not include information on the horizontal density gradient between the littoral and interior regions, and could thus be calculated based on the forcing conditions (B_0, u_*) and h_{SML}. This is the advantage of using χ_{MO} since the latter information can simply be inferred from one single mooring deployed in a lake.

4.3 Applicability framework

The mathematical expression in Eq. 8 is expected to work as long as (i) (quasi-)steady conditions are reached, (ii) wind stress and convection are the main sources of turbulence and water motions in the lake, and (iii) Coriolis effects are negligible. The convective scaling in Eq. (1) already implies a steady thermal balance and an equilibrium between the inertial advective term and the pressure gradient term in the cross-shore momentum equation, that is:

$$u\frac{\partial u}{\partial x} \approx \frac{1}{\rho_0}\frac{\partial p}{\partial x}, \qquad (12)$$

$$u\frac{\partial \bar{T}}{\partial x} \approx \frac{Q_o}{\rho_0 c_p\, D(x)}, \qquad (13)$$

where p ($\approx \alpha g \rho_0 \bar{T} D(x)$) is pressure and $\bar{T}$ is a depth-averaged temperature. Monismith et al. (2006) studied the exchange flows due to differential cooling in a coral reef in Israel. They showed, by nondimensionalizing the governing momentum and buoyancy equations, that neglecting the unsteady/inertial term $\partial u/\partial t$ is a reasonable assumption as long as ($h_{SML}\, S^{-2/3}\, P^{-1}\, w_*^{-1}$) << 1, P being the period of the thermal forcing (heating/cooling cycle). In our simulations, where a constant cooling rate is applied ($P \rightarrow \infty$), this condition is met. In Rotsee, at the time when TSs were observed (July to December), h_{SML} ranged from 2 m to 16 m, and average w_* from 5×10^{-3} to 6.5×10^{-3} m s^{-1} (Doda et al., 2021). For S = 0.03 and a 24 h cooling cycle, the term ($h_{SML}\, S^{-2/3}\, P^{-1}\, w_*^{-1}$) remained always < 0.4 and Doda et al. (2021) showed that Eq. (1) successfully predicted cross-shore flows in the lake during TS events. However, this condition may not be met in deeper littoral regions, with lower slopes, lower surface buoyancy fluxes, and/or shorter cooling periods (e.g, Molina et al., 2014), where flow dynamics may follow an inertial-viscous buoyancy balance (e.g. Farrow, 2013; Farrow & Patterson, 1993; Lin, 2015; Ulloa et al., 2018).

The viscous term ($\nu_z \partial^2 u/\partial z^2$) could be discarded in low energetic environments, when the characteristic shear velocity is O(w_*) (e.g., Monismith et al., 2006). In this study, the viscous term contributes to the exchange flows once wind stress acts on the lake surface. However, strong background currents (e.g., alongshore currents, Ulloa et al., 2018) and/or high bed roughness, for example, could also contribute to this term. In our scaling, we also consider that mild winds do not lead to strong tilting of the isotherms. Assuming a two-layer stratified system, the expected displacement $\Delta h/h_T$ can be estimated from the Wedderburn number W as (Shintani et al., 2010) $\Delta h/h_T = 1-[2\, \pi^{-1} \tan^{-1}(9/8\, W-1)^{0.81}]^{0.57}$, where $W = g' h_T^2 u_*^{-2} L^{-1}$, and g' (= $g\, (\rho_2-\rho_1)\, \rho_2^{-1}$) is the reduced gravity calculated with the bottom-layer (ρ_2) and top-layer (ρ_1) densities. Thus, mild winds could still lead to upwelling events in long lakes (large L) with shallow thermoclines (small h_T) and/or weak stratification (small g').

For a Coriolis frequency of ~ 1.1×10^{-4} s^{-1} as in Rotsee and maximum offshore radial velocities $u_{r\text{-}max}$ of 0.03 m s^{-1} for the zero wind stress case (Fig. 2), the Rossby number in our simulations, $Ro = u_{r\text{-}max}\, (f\, L_{SML})^{-1}$, is ~1 and Coriolis acceleration should not affect the trajectories of the downslope density currents before intruding at the base of the mixed layer. Moreover, we tested the interaction of TS with cross-shore winds, so that wind-driven currents do not contribute to the Coriolis-acceleration term, vf, in the cross-shore momentum equation. Studies in oceanic littoral regions have shown, however, that strong alongshore tidally-driven (Ulloa et al., 2018) or wind-driven currents (e.g., Lentz & Fewings, 2012; Wu et al., 2018) could also affect cross-shore flows via Coriolis acceleration.

5 Conclusions

Cross-shore water exchanges control the residence time of the different compounds in the littoral region of lakes. The mechanisms responsible for these horizontal exchanges have been traditionally investigated separately even though most of the time lake dynamics result from a combination of different forcings. This study takes a step in that direction by analyzing the effect of the interaction of differential cooling and wind-driven currents on cross-shore discharges within the surface mixed layer of enclosed stratified basins. We have proposed a practical mathematical expression of the form $q_{total} = q_c + q_w$ that accounts for the cooling- (q_c) and wind-driven (q_w) contributions for the net cross-shore discharge. This expression is shown to improve cross-shore discharge predictions in the littoral region of lakes with negligible alongshore currents and under (quasi-)steady forcing conditions and cross-shore directed winds. We suggest using this parameterization in a well-defined range of non-dimensional Monin Obukhov length scale $0.1 \lesssim \chi_{MO} \lesssim 0.5$.

Acknowledgments

MITgcm input files used in this study and data displayed in the figures can be accessed at (temporary link for initial submission: https://drive.switch.ch/index.php/s/8bn53z2IKOHxHet). This work was supported by the Swiss National Science Foundation (project Buoyancy driven nearshore transport in lakes, HYPOlimnetic THErmal SIphonS, HYPOTHESIS, reference 175919). Computer resources were provided by the Swiss National Supercomputing Centre.

References

Bengtsson, L. (1973). Conclusions about turbulent exchange coefficients from model studies. *Hydrological Sciences Journal/Journal Des Sciences Hydrologiques*, *109*(1), 306–312.

Bengtsson, L. (1978). Wind induced circulation in lakes. *Nord Hydrol*, *9*(2), 75–94. https://doi.org/10.2166/nh.1978.0007

Biton, E., Silverman, J., & Gildor, H. (2008). Observations and modeling of a pulsating density current. *Geophysical Research Letters*, *35*(14), L14603. https://doi.org/10.1029/2008GL034123

Bonvin, F., Rutler, R., Chavre, N., Halder, J., & Kohn, T. (2011). Spatial and temporal presence of a wastewater-derived micropollutant plume in Lake Geneva. *Environmental Science and Technology*, *45*(11), 4702–4709. https://doi.org/10.1021/es2003588

Carpenter, S. R., Caraco, N. F., Correll, D. L., Howarth, R. W., Sharpley, A. N., & Smith, V. H. (1998). Nonpoint Pollution of Surface Waters with Phosphorus and Nitrogen. *Ecological Applications*, *8*(3), 559–568. https://doi.org/10.1890/1051-0761(1998)008[0559:NPOSWW]2.0.CO;2

Coman, M. A., & Wells, M. G. (2012). An oscillating bottom boundary layer connects the littoral and pelagic regions of Lake Opeongo, Canada. *Water Quality Research Journal of Canada*, *47*(3–4), 215. https://doi.org/10.2166/wqrjc.2012.039

Cormack, D. E., Stone, G. P., & Leal, L. G. (1975). The effect of upper surface conditions on convection in a shallow cavity with differentially heated end-walls. *International Journal of Heat and Mass Transfer*, *18*(5), 635–648. https://doi.org/10.1016/0017-9310(75)90275-6

Cortés, A., Fleenor, W. E., Wells, M. G., de Vicente, I., & Rueda, F. J. (2014). Pathways of river water to the surface layers of stratified reservoirs. *Limnology and Oceanography*, *59*(1), 233–250. https://doi.org/10.4319/lo.2014.59.1.0233

Cyr, H., McCabe, S. K., & Nürnberg, G. K. (2009). Phosphorus sorption experiments and the potential for internal phosphorus loading in littoral areas of a stratified lake. *Water Research*, *43*(6), 1654–1666. https://doi.org/10.1016/j.watres.2008.12.050

Deardorff, J. W. (1970). Convective Velocity and Temperature Scales for the Unstable Planetary Boundary Layer and for Rayleigh Convection. *Journal of the Atmospheric Sciences*, *27*(8), 1211–1213. https://doi.org/10.1175/1520-0469(1970)027<1211:cvatsf>2.0.co;2

Doda, T., Ramón, C. L., Ulloa, H. N., Wüest, A., & Bouffard, D. (2021). Seasonality of density currents induced by differential cooling. *Hydrol. Earth Syst. Sci. Discuss. [Preprint], in*

Review. https://doi.org/10.5194/hess-2021-195

Farrow, D. E. (2013). Periodically driven circulation near the shore of a lake. *Environmental Fluid Mechanics*, *13*(3), 243–255. https://doi.org/10.1007/s10652-012-9261-4

Farrow, D. E., & Patterson, J. C. (1993). On the response of a reservoir sidearm to diurnal heating and cooling. *Journal of Fluid Mechanics*, *246*(1), 143. https://doi.org/10.1017/S0022112093000072

Fer, I., Lemmin, U., & Thorpe, S. A. (2001). Cascading of water down the sloping sides of a deep lake in winter. *Geophysical Research Letters*, *28*(10), 2093–2096. https://doi.org/10.1029/2000GL012599

Fer, I., Lemmin, U., & Thorpe, S. A. (2002). Winter cascading of cold water in Lake Geneva. *Journal of Geophysical Research*, *107*(C6), 3060. https://doi.org/10.1029/2001JC000828

Fitchko, J., & Hutchinson, T. C. (1975). A Comparative Study of Heavy Metal Concentrations in River Mouth Sediments Around the Great Lakes. *Journal of Great Lakes Research*, *1*(1), 46–78. https://doi.org/10.1016/S0380-1330(75)72335-3

Haas, M., Baumann, F., Castella, D., Haghipour, N., Reusch, A., Strasser, M., et al. (2019). Roman-driven cultural eutrophication of Lake Murten, Switzerland. *Earth and Planetary Science Letters*, *505*, 110–117. https://doi.org/10.1016/j.epsl.2018.10.027

Harashima, A., & Watanabe, M. (1986). Laboratory experiments on the steady gravitational circulation excited by cooling of the water surface. *Journal of Geophysical Research*, *91*(C11), 13056. https://doi.org/10.1029/jc091ic11p13056

Hofmann, H. (2013). Spatiotemporal distribution patterns of dissolved methane in lakes: How accurate are the current estimations of the diffusive flux path? *Geophysical Research Letters*, *40*(11), 2779–2784. https://doi.org/10.1002/grl.50453

Hofmann, H., Federwisch, L., & Peeters, F. (2010). Wave-induced release of methane: Littoral zones as source of methane in lakes. *Limnology and Oceanography*, *55*(5), 1990–2000. https://doi.org/10.4319/lo.2010.55.5.1990

Hogg, C. A. R., Marti, C. L., Huppert, H. E., & Imberger, J. (2013). Mixing of an interflow into the ambient water of Lake Iseo. *Limnology and Oceanography*, *58*(2), 579–592. https://doi.org/10.4319/lo.2013.58.2.0579

Horwitz, R., & Lentz, S. J. (2014). Inner-shelf response to cross-shelf wind stress: The importance of the cross-shelf density gradient in an idealized numerical model and field observations. *Journal of Physical Oceanography*, *44*(1), 86–103. https://doi.org/10.1175/JPO-D-13-075.1

James, W. F., & Barko, J. W. (1991). Estimation of phosphorus exchange between littoral and pelagic zones during nighttime convective circulation. *Limnology and Oceanography*, *36*(1), 179–187. https://doi.org/10.4319/lo.1991.36.1.0179

James, W. F., Barko, J. W., & Eakin, H. L. (1994). Convective water exchanges during differential cooling and heating: implications for dissolved constituent transport. *Hydrobiologia*, *294*(2), 167–176. https://doi.org/10.1007/BF00016857

Kandie, F. J., Krauss, M., Beckers, L. M., Massei, R., Fillinger, U., Becker, J., et al. (2020). Occurrence and risk assessment of organic micropollutants in freshwater systems within the Lake Victoria South Basin, Kenya. *Science of the Total Environment*, *714*, 136748. https://doi.org/10.1016/j.scitotenv.2020.136748

Lentz, S. J., & Fewings, M. R. (2012). The wind- and wave-driven inner-shelf circulation. *Annual Review of Marine Science*, *4*, 317–343. https://doi.org/10.1146/annurev-marine-120709-142745

Li, J., Liu, H., & Paul Chen, J. (2018). Microplastics in freshwater systems: A review on occurrence, environmental effects, and methods for microplastics detection. *Water Research*. Elsevier Ltd. https://doi.org/10.1016/j.watres.2017.12.056

Lin, Y.-T. (2015). Wind effect on diurnal thermally driven flow in vegetated nearshore of a lake. *Environmental Fluid Mechanics*, *15*(1), 161–178. https://doi.org/10.1007/s10652-014-9368-x

Mahjabin, T., Pattiaratchi, C., & Hetzel, Y. (2019). Wind effects on dense shelf water cascades in south-west Australia. *Continental Shelf Research*, *189*, 103975. https://doi.org/10.1016/j.csr.2019.103975

Mahjabin, T., Pattiaratchi, C., & Hetzel, Y. (2020). Occurrence and seasonal variability of Dense Shelf Water Cascades along Australian continental shelves. *Scientific Reports*, *10*(1), 1–13. https://doi.org/10.1038/s41598-020-66711-5

Mao, Y., Lei, C., & Patterson, J. C. (2019). Natural convection in a reservoir induced by sinusoidally varying temperature at the water surface. *International Journal of Heat and Mass Transfer*, *134*, 610–627. https://doi.org/10.1016/J.IJHEATMASSTRANSFER.2019.01.071

Marshall, J., Adcroft, A., Hill, C., Perelman, L., & Heisey, C. (1997). A finite-volume, incompressible Navier Stokes model for studies of the ocean on parallel computers. *Journal of Geophysical Research: Oceans*, *102*(C3), 5753–5766. https://doi.org/10.1029/96JC02775

Marshall, J., Hill, C., Perelman, L., & Adcroft, A. (1997). Hydrostatic, quasi-hydrostatic, and nonhydrostatic ocean modeling. *Journal of Geophysical Research: Oceans*, *102*(C3), 5733–5752. https://doi.org/10.1029/96JC02776

Marti, C. L., & Imberger, J. (2008). Exchange between littoral and pelagic waters in a stratified lake due to wind-induced motions: Lake Kinneret, Israel. *Hydrobiologia*, *603*(1), 25–51. https://doi.org/10.1007/s10750-007-9243-6

McDougall, T. J., Jackett, D. R., Wright, D. G., & Feistel, R. (2003). Accurate and Computationally Efficient Algorithms for Potential Temperature and Density of Seawater. *Journal of Atmospheric and Oceanic Technology*, *20*(5), 730–741. https://doi.org/10.1175/1520-0426(2003)20<730:AACEAF>2.0.CO;2

Molina, L., Pawlak, G., Wells, J. R., Monismith, S. G., & Merrifield, M. A. (2014). Diurnal cross-shore thermal exchange on a tropical forereef. *Journal of Geophysical Research: Oceans*, *119*(9), 6101–6120. https://doi.org/10.1002/2013JC009621

Monismith, S. G., Imberger, J., & Morison, M. L. (1990). Convective motions in the sidearm of a small reservoir. *Limnology and Oceanography*, *35*(8), 1676–1702.

https://doi.org/10.4319/lo.1990.35.8.1676

Monismith, S. G., Genin, A., Reidenbach, M. A., Yahel, G., Koseff, J. R., Monismith, S. G., et al. (2006). Thermally Driven Exchanges between a Coral Reef and the Adjoining Ocean. *Journal of Physical Oceanography*, *36*(7), 1332–1347. https://doi.org/10.1175/JPO2916.1

Park, H.-K., Byeon, M.-S., Shin, Y.-N., & Jung, D.-I. (2009). Sources and spatial and temporal characteristics of organic carbon in two large reservoirs with contrasting hydrologic characteristics. *Water Resources Research*, *45*(11). https://doi.org/10.1029/2009WR008043

Perazzolo, C., Morasch, B., Kohn, T., Magnet, A., Thonney, D., & Chèvre, N. (2010). Occurrence and fate of micropollutants in the Vidy Bay of Lake Geneva, Switzerland. Part I: Priority list for environmental risk assessment of pharmaceuticals. *Environmental Toxicology and Chemistry*, *29*(8), n/a-n/a. https://doi.org/10.1002/etc.221

Phillips, O. M. (1966). On turbulent convection currents and the circulation of the Red Sea. *Deep-Sea Research and Oceanographic Abstracts*, *13*(6), 1149–1160. https://doi.org/10.1016/0011-7471(66)90706-6

Ramón, C. L., Ulloa, H. N., Doda, T., Winters, K. B., & Bouffard, D. (2021). Bathymetry and latitude modify lake warming under ice. *Hydrology and Earth System Sciences*, *25*(4), 1813–1825. https://doi.org/10.5194/hess-25-1813-2021

Rao, Y. R., & Schwab, D. J. (2007). Transport and Mixing Between the Coastal and Offshore Waters in the Great Lakes: a Review. *Journal of Great Lakes Research*, *33*(1), 202–218. https://doi.org/10.3394/0380-1330(2007)33[202:TAMBTC]2.0.CO;2

Read, J. S., Hamilton, D. P., Desai, A. R., Rose, K. C., MacIntyre, S., Lenters, J. D., et al. (2012). Lake-size dependency of wind shear and convection as controls on gas exchange. *Geophysical Research Letters*, *39*(9), n/a-n/a. https://doi.org/10.1029/2012GL051886

Roget, E., Colomer, J., Casamitjana, X., & Llebot, J. E. (1993). Bottom currents induced by baroclinic forcing in Lake Banyoles (Spain). *Aquatic Sciences*, *55*(3), 206–227. https://doi.org/10.1007/BF00877450

Rueda, F. J., Moreno-Ostos, E., & Cruz-Pizarro, L. (2007). Spatial and temporal scales of transport during the cooling phase of the ice-free period in a small high-mountain lake. *Aquatic Sciences*, *69*(1), 115–128. https://doi.org/10.1007/s00027-006-0823-8

Santiago-Mandujano, F., & Firing, E. (1990). Mixed-layer shear generated by wind stress in the central equatorial Pacific. *Journal of Physical Oceanography*, *20*, 1576–1582. https://doi.org/10.1175/1520-0485(1990)020<1576:MLSGBW>2.0.CO;2.

Shapiro, G. I., Huthnance, J. M., & Ivanov, V. V. (2003). Dense water cascading off the continental shelf. *Journal of Geophysical Research*, *108*(C12), 3390. https://doi.org/10.1029/2002JC001610

Shintani, T., de la Fuente, A., de la Fuente, A., Niño, Y., & Imberger, J. (2010). Generalizations of the Wedderburn Number: Parameterizing Upwelling in Stratified Lakes. *Limnology and Oceanography*, *55*(3), 1377–1389. https://doi.org/10.4319/lo.2010.55.3.1377

Sighicelli, M., Pietrelli, L., Lecce, F., Iannilli, V., Falconieri, M., Coscia, L., et al. (2018). Microplastic pollution in the surface waters of Italian Subalpine Lakes. *Environmental Pollution*, *236*, 645–651. https://doi.org/10.1016/j.envpol.2018.02.008

Sturman, J. J., & Ivey, G. N. (1998). Unsteady convective exchange flows in cavities. *Journal of Fluid Mechanics*, *368*, S002211209800175X. https://doi.org/10.1017/S002211209800175X

Sturman, J. J., Oldham, C. E., & Ivey, G. N. (1999). Steady convective exchange flows down slopes. *Aquatic Sciences*, *61*(3), 260. https://doi.org/10.1007/s000270050065

Thevenon, F., Graham, N. D., Chiaradia, M., Arpagaus, P., Wildi, W., & Poté, J. (2011). Local to regional scale industrial heavy metal pollution recorded in sediments of large freshwater lakes in central Europe (lakes Geneva and Lucerne) over the last centuries. *Science of the Total Environment*, *412–413*, 239–247. https://doi.org/10.1016/j.scitotenv.2011.09.025

Timoshkin, O. A., Moore, M. V., Kulikova, N. N., Tomberg, I. V., Malnik, V. V., Shimaraev, M. N., et al. (2018). Groundwater contamination by sewage causes benthic algal outbreaks in the littoral zone of Lake Baikal (East Siberia). *Journal of Great Lakes Research*, *44*(2), 230–244. https://doi.org/10.1016/j.jglr.2018.01.008

Ulloa, H. N., Davis, K. A., Monismith, S. G., & Pawlak, G. (2018). Temporal variability in thermally driven cross-shore exchange: The role of semidiurnal tides. *Journal of Physical Oceanography*, *48*(7), 1513–1531. https://doi.org/10.1175/JPO-D-17-0257.1

Ulloa, H. N., Ramón, C. L., Doda, T., Wüest, A., & Bouffard, D. (2021). Development of overturning circulation due to surface cooling in sloping waterbodies. *Under Review in Journal of Fluid Mechanics* (https://enacshare.epfl.ch/bwtmuhWFixVv4oyX7HAJ3).

Verburg, P., Antenucci, J. P., & Hecky, R. E. (2011). Differential cooling drives large-scale convective circulation in Lake Tanganyika. *Limnology and Oceanography*, *56*(3), 910–926. https://doi.org/10.4319/lo.2011.56.3.0910

Wei, J., Duan, M., Li, Y., Nwankwegu, A. S., Ji, Y., & Zhang, J. (2019). Concentration and pollution assessment of heavy metals within surface sediments of the Raohe Basin, China. *Scientific Reports*, *9*(1), 1–7. https://doi.org/10.1038/s41598-019-49724-7

Winters, K. B., Lombard, P. N., Riley, J. J., & D’Asaro, E. A. (1995). Available potential energy and mixing in density-stratified fluids. *Journal of Fluid Mechanics*, *289*, 115–128. https://doi.org/10.1017/S002211209500125X

Woodward, B. L., Marti, C. L., Imberger, J., Hipsey, M. R., & Oldham, C. E. (2017). Wind and buoyancy driven horizontal exchange in shallow embayments of a tropical reservoir: Lake Argyle, Western Australia. *Limnology and Oceanography*, *62*(4), 1636–1657. https://doi.org/10.1002/lno.10522

Wu, X., Cahl, D., & Voulgaris, G. (2018). Effects of wind stress and surface cooling on cross-shore exchange. *Journal of Physical Oceanography*, *48*(11), 2627–2647. https://doi.org/10.1175/JPO-D-17-0216.1

Wüest, A., & Lorke, A. (2003). Small-scale hydrodynamics in lakes. *Annual Review of Fluid Mechanics*, *35*(1), 373–412. https://doi.org/10.1146/annurev.fluid.35.101101.161220

Yakimovich, K. M., Orland, C., Emilson, E. J. S., Tanentzap, A. J., Basiliko, N., & Mykytczuk, N. C. S. (2020). Lake characteristics influence how methanogens in littoral sediments respond to terrestrial litter inputs. *ISME Journal*, *14*(8), 2153–2163.

https://doi.org/10.1038/s41396-020-0680-9

Water Resources Research

Supporting Information for

Flushing the Lake Littoral Region: the Interaction of Differential Cooling and Mild Winds

Cintia L. Ramón,[1,2*], Hugo N. Ulloa[3,4], Tomy Doda[1,4], and Damien Bouffard[1]

[1]Department of Surface Waters – Research and Management, Eawag (Swiss Federal Institute of Aquatic Science and Technology), Kastanienbaum, Switzerland.

[2]Water Research Institute and Department of Civil Engineering, University of Granada, Spain.

[3]Department of Earth and Environmental Science, University of Pennsylvania, Philadelphia, USA

[4]Physics of Aquatic Systems Laboratory, EPFL (École Polytechnique Fédérale de Lausanne), Lausanne, Switzerland.

Contents of this file

Figures S1 to S2

Introduction

This Supporting Information includes two figures. Figure S1 shows the modeled unit-width discharges in the downwind littoral region for W-runs in Table 1, where the lake was only forced with a surface wind stress. It also shows the fit of the modeled discharges to Eq. 7 (scaling for wind-driven unit-width discharges). Figure S2 compares the horizontal Richardson number Ri_x (Eq. 9) with χ_{MO} (Eq. 2).

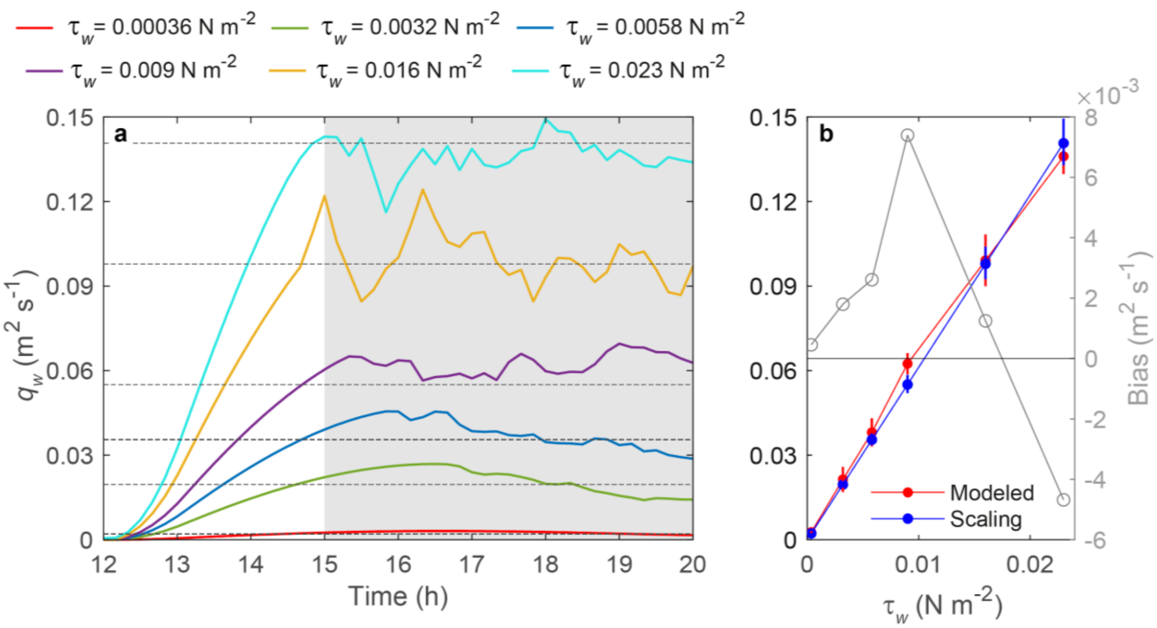

Figure S1. Scaling for wind-driven unit-width discharges. (a) Time signal of offshore modeled flows in the downwind side (profile D) for the W-runs in Table 1, and (b) time-averaged modeled unit-width discharges and best-fit scaling (Eq. 7). The period for time averaging (gray-shaded area in (a)) was chosen from one-half of the internal wave period from the start of the forcing until ~20 h when the flow remained quasi-steady. Dotted lines in (a) show the predicted flows using Eq. 7. Vertical lines in the modeled and scaled values in (b) show ± one standard deviation and 95% confidence interval. Best fit (R^2 = 0.993) was achieved for $\nu_z = 6.06 \times 10^{-4} \pm 3.6 \times 10^{-5}$ m^2 s^{-1}.

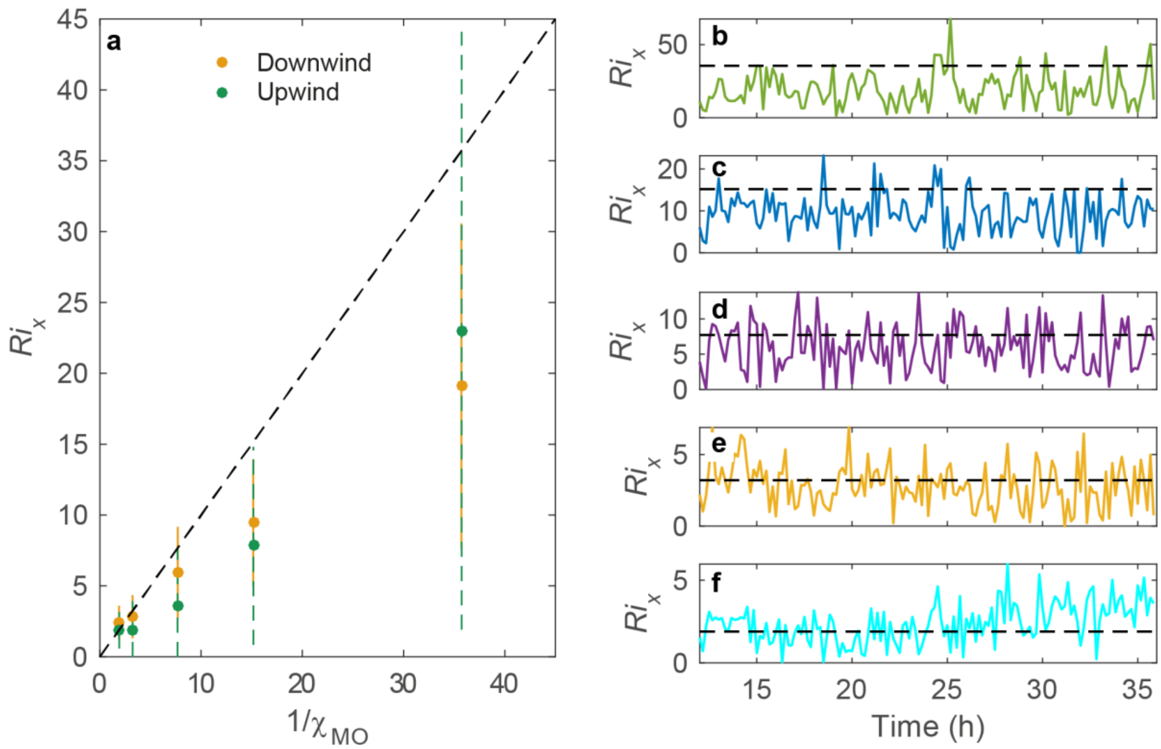

Figure S2. Relationship between Ri_x (Eq. 9) and χ_{MO} (Eq. 2). (a) Time-averaged horizontal Richardson number Ri_x versus χ_{MO}^{-1} for runs 2 to 6 in Table 1. Vertical lines show ± one standard deviation of Ri_x and the black dashed line the 1:1 relationship. (b-f) Time series of Ri_x in the downwind region for (b) run 2 (χ_{MO} = 0.028), (c) run 3 (χ_{MO} = 0.066), (d) run 4 (χ_{MO} = 0.13), (e) run 5 (χ_{MO} = 0.31) and (f) run 6 (χ_{MO} = 0.53). Black dashed lines in b-f show χ_{MO}^{-1}. Ri_x was calculated with the average horizontal density gradient within the littoral region and the littoral region's average depth (h_{lit}).